# COMPUTATIONAL FLUID DYNAMICS FOR SIMULATION OF A GAS-LIQUID FLOW ON A SIEVE PLATE: MODEL COMPARISONS

**Cíntia Soares*, Dirceu Noriler*, António André Chivanga Barros**, Henry França Meier** and Maria Regina Wolf Maciel***

* Laboratory of Separation Process Development – Chemical Engineering School – State University of Campinas (UNICAMP) – P.O. Box: 6066 – Zip Code: 13081-970 – Campinas – SP – Brazil
E-mail: wolf@feq.unicamp.br and scynthia@feq.unicamp.br
** Chemical Engineering Department – Regional University of Blumenau (FURB) Blumenau – SC – Brazil
E-mail: chivanga@furb.br and meier@furb.br

## ABSTRACT

Abstract: The aim of this work is to present the turbulent flow simulations on a sieve plate and to carry out a comparison between two different models. The first one is based on the assumption that the liquid flow is more important than the gas flow and the second model assumes the 3-D two phase flow with the homogeneous model hypothesis. A commercial CFD code (CFX 4.4) was used, and was possible to conclude that the single phase model is highly dependent on empirical parameters, what represents a limitation of the model, and that the 3-D two-phase model makes possible the visualisation of the asymmetry of the flow on the tray.

## INTRODUCTION

Distillation columns are one of the most important separation techniques. A considerable quantity of research related with development of models to represent the real behaviour of a distillation column has been developed. Despite the relevant results obtained with the equilibrium and the nonequilibrium stage models, they neglect all fluid dynamics phenomena by assumption of the perfect mixture. However, it has long been recognised that the liquid flow pattern on a distillation tray is of large importance on the mass transfer efficiency, and this influence only can be analysed making a fluid dynamic study.

Recently, advances and interest in the use of CFD techniques have allowed the study of fluid dynamic of distillation tray. The evaluation of flow patterns on a sieve plate has been realised considering different assumptions to describe the fluid

dynamic behaviour of the vapour-liquid flow. Mehta *et al.* [1] have analysed the liquid phase flow patterns on a sieve tray by solving the time-averaged equations of continuity of mass and momentum only for the liquid phase. Interactions with the vapour phase were taken into account through the use of interface momentum transfer coefficients determined from empirical correlations. Liu *et al*. [2] presented experimental and numerical studies to evaluate a two-dimensional model for predicting velocity fields and turbulent properties describing the liquid-phase flow on sieve tray with the consideration that both, the resistance and the bubbling effects, created by the uprising vapour.

van Baten *et al.* [3] developed a three-dimensional transient CFD model for describing hydrodynamics of sieve trays, modelling the gas and the liquid phases in the Eulerian framework as two interpenetrating phases.

Despite the simplicity of the empirical model proposed by Liu *et al.* [2] to predict the generation of turbulence in function of the cross flow of bubbles in the liquid phase, it presents a linear relation between generation of turbulence and pressure drop. The model is largely dependent on the $C_e$ linear parameter and needs to be well adjusted [4].

Based on this fact, this work presents the 3-D two phase homogeneous model and the turbulent flow simulations on a bubble column and on a sieve tray, obtained through computational fluid dynamic techniques. The results were compared with the single phase model. In this study the water-air system was used in both simulations. The single phase model is based on the assumption that the liquid flow is more important than the gas flow, and an averaged flow was modelled as a single phase (only liquid phase), with influence of the bubbling of the gas phase by mean of a resistive force and an additional turbulence caused by bubbles. Liquid flow with radial symmetry and no thermal effects on the liquid flow were supposed. The 3-D two phase flow with the homogeneous hypothesis (3-D homogeneous two phase model) is a simplification of the heterogeneous model, and it assumes that transported quantities are the same for all phases. However, the volume fractions are still assumed distinct. The standard k-$\varepsilon$ turbulence model was used with the introduction of an additional term related to the turbulence due to the gas bubbling across the liquid phase. Finite volume method was applied to solve the partial differential equation of the model, with some particularities such as SIMPLEC algorithms for pressure-velocity coupling, body fitted in a generalised co-ordinate system for grid generation, under-relaxation and false time step for stability and convergence, among others. A commercial CFD code CFX 4.4 of AEA Technology, Harwell, UK, was also used as pre-processor, solver and post-processor in all case studies. The numerical results allowed the description of the tray hydrodynamics in several operating conditions.

## MATHEMATICAL MODELLING

### Governing Equations

The three-dimensional, transient, turbulent and multiphase model in Cartesian co-ordinate system for any property in a general phase k ,$\phi_k$, can be generalised by the following equation:

$$\frac{\partial(\rho_k f_k \phi_k)}{\partial t} + \frac{\partial}{\partial x}(\rho_k f_k v_x \phi_k) + \frac{\partial}{\partial y}(\rho_k f_k v_y \phi_k) + \frac{\partial}{\partial z}(\rho_k f_k v_z \phi_k) = -\frac{\partial}{\partial x}\left[f_k \Gamma_k \frac{\partial(\rho_k \phi_k)}{\partial x}\right] - \frac{\partial}{\partial y}\left[f_k \Gamma_k \frac{\partial(\rho_k \phi_k)}{\partial y}\right] - \frac{\partial}{\partial z}\left[f_k \Gamma_k \frac{\partial(\rho_k \phi_k)}{\partial z}\right] + S_\phi \quad (1)$$

where $\phi_k$ are the fluid dynamic properties (u, v, w, k and $\varepsilon$) in the *k* phase, and $\Gamma$ and S are the diffusion coefficient and the source term for each property $\phi_k$, respectively.

The left hand side gives the transient and the net convective flux and the right hand side contains the net diffusive flux and generation or destruction of the property $\phi_k$.

Based on the generalised Equation (1), the following models will be developed:

- 2-D Single Phase Model (2-DSM)
- 3-D Two Phase Homogeneous Model (3-DTHomM)

At following details of each model are presented.

**2-D Single Phase Model (2-DSM)**
The main assumption imposed to idealise the physical situation and to describe mathematically the fluid dynamic of the flow on a distillation tray are:

- the liquid flow is more important than the gas flow; the averaged flow can be modelled as a single phase (just the liquid phase), with influence of the bubbling of the gas phase by means of resistive force and of additional turbulence provoked by the bubbles;
- liquid flow can be supposed with radial symmetry planes, making possible to consider the geometry as one semi-infinity slab in a rectangular co-ordinate system;
- thermal effects have no influence in the liquid flow;
- the flow has a stable steady state.

The 2-DSM model makes possible the evaluation of resisting force from the vapour phase to the liquid phase and also the bubbling action on the turbulence characteristics of the flow, by introduction of two constitutive equations: one for resistive force between phases [5]; and another for generation of turbulent energy due to the bubbling action of the vapour phase [6]. The model is largely dependent on an empirical parameter, denoted by transfer coefficient ($C_e$), responsible for increasing the turbulence generation in the k-$\varepsilon$ model, due to bubbling effects of the vapour phase on the liquid phase.

Table 1 presents the compact form of the 2-DSM model defining the source terms for each variable $\phi_k$, $S_{\phi k}$, and the expressions for the diffusion coefficients $\Gamma$, according to Equation (1).

*Table 1. Compact form of the 2-D single phase model.*

| Conservation | $f_k$ | $\phi_k$ | $\Gamma_k$ | $S_{\phi_k}$ |
|---|---|---|---|---|
| Mass | 1 | 1 | 0 | 0 |
| Momentum Direction x | 1 | $v_x$ | $\frac{\mu^{eff}}{\rho}$ | $f_x - \frac{\partial p}{\partial x}$ |
| Momentum Direction y | 1 | $v_y$ | $\frac{\mu^{eff}}{\rho}$ | $f_y - \frac{\partial p}{\partial y}$ |
| Momentum Direction z | - | - | - | - |
| Turbulent Kinetic Energy | 1 | k | $\frac{\mu + \frac{\mu^t}{\sigma^k}}{\rho}$ | $G_T - \rho\varepsilon$ |
| Dissipation Rate of Turbulent Kinetic Energy | 1 | $\varepsilon$ | $\frac{\mu + \frac{\mu^t}{\sigma^\varepsilon}}{\rho}$ | $\frac{\varepsilon}{k}\left(C_1 G_T - C_2 \rho\varepsilon\right)$ |

Constitutive Equations

$$f_x = -\frac{\rho_g u_s}{h_w} v_x \qquad f_y = -\frac{\rho_g u_s}{h_w} v_y \qquad G_T = G_{T1} + G_{T2}$$

$$G_{T1} = \mu^t \left[ 2\left(\frac{\partial v_x}{\partial x}\right)^2 + 2\left(\frac{\partial v_x}{\partial y}\right)^2 + \left(\frac{\partial v_x}{\partial y} + \frac{\partial v_y}{\partial x}\right)^2 \right] \qquad G_{T2} = C_e \frac{\Delta P\, u_s}{h}$$

$$\mu^{(t)} = C_\mu \cdot \frac{k^2}{\varepsilon}$$

$C_1$, $C_2$, $C_\mu$ model constants $C_e$ transfer coefficient

**Boundary Conditions for 2-DSM Model**

Due to the elliptical characteristic of the partial differential equations of the model, boundary conditions at all frontiers of the physical domain are necessary: at the inlet, uniform profile of velocities and turbulent properties are imposed; symmetry conditions were imposed for all dynamic variables at the centre line of the tray; non slip conditions on the wall and pressure condition in the outlet of the liquid were also applied for all variables. These conditions can be written in a mathematical form according to Table 2.

*Table 2 – Boundary conditions for the 2-DSM model.*

| Boundary Condition | Phase | |
|---|---|---|
| | Liquid | Gas |
| Inlet | $v_x\|_{x=0} = \frac{L}{h}\ \ v_y\|_{x=0} = 0$ <br> $k\|_{x=0.} = 0.003\left(v_x\|_{x=0}\right)^2$ <br> $\varepsilon\|_{x=0} = \frac{0.09\left(k\|_{x=0}\right)^{3/2}}{0.03\,W/2}$ | - |
| Outlet (Pressure) | $\left.\frac{\partial v_x}{\partial y}\right\|_{out} = \left.\frac{\partial v_y}{\partial y}\right\|_{out} = \left.\frac{\partial k}{\partial y}\right\|_{out} = \left.\frac{\partial \varepsilon}{\partial y}\right\|_{out} = 0$ | - |
| Wall | $v_x\|_{wall} = v_y\|_{wall} = k\|_{wall} = \left.\frac{\partial \varepsilon}{\partial y}\right\|_{wall} = 0$ <br> (non-slip) | - |
| Symmetry | $\left.\frac{\partial v_x}{\partial y}\right\|_{y=0} = \left.\frac{\partial k}{\partial y}\right\|_{y=0} = \left.\frac{\partial \varepsilon}{\partial y}\right\|_{y=0} = v_y = 0$ | - |

Figure 1 shows the geometry and the location of all boundaries used in the 2-D model for the sieve plate case.

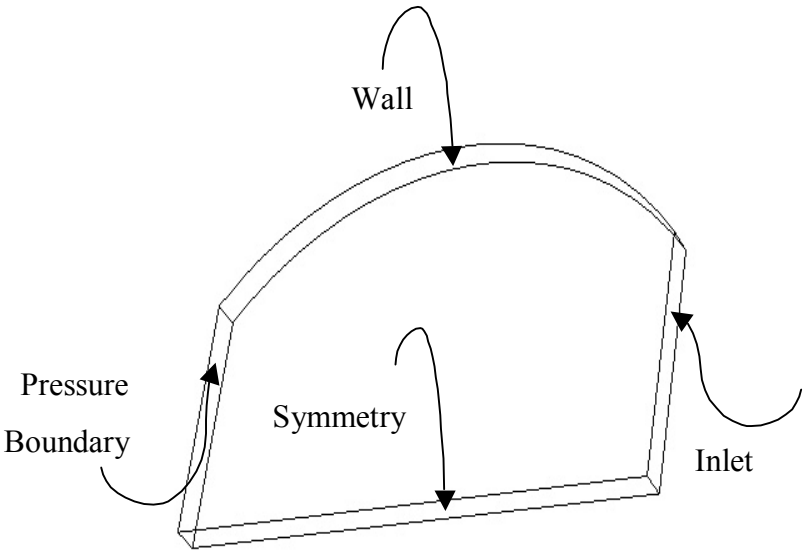


*Figure 1. Schematic distillation tray and its physical domain.*

**3-D Two Phase Homogeneous Model (3-DTHM)**

The homogeneous model is a simplification of the multi-fluid model. It assumes that the transported properties are the same for all phases, i.e.

$$\phi_k = \phi \qquad 1 \le k \le N_k \qquad (2)$$

however, the volume fractions are still assumed distinct.

*Table 3. Compact form of the 3-D homogeneous model.*

| Conservation | $f_k$ | $\phi_k$ | $\Gamma_k$ | $S_\phi$ |
|---|---|---|---|---|
| Mass Liquid Phase | $f_l$ | 1 | 0 | 0 |
| Mass Vapour Phase | $f_g$ | 1 | 0 | 0 |
| Momentum Direction x | 1 | $v_x$ | $\frac{\mu_{mix}+\mu^t}{\rho_{mix}}$ | $-\frac{\partial p}{\partial x}+\rho_{mix}g_x+Fs_x$ |
| Momentum Direction y | 1 | $v_y$ | $\frac{\mu_{mix}+\mu^t}{\rho_{mix}}$ | $-\frac{\partial p}{\partial y}+\rho_{mix}g_y+Fs_y$ |
| Momentum Direction z | 1 | $v_z$ | $\frac{\mu_{mix}+\mu^t}{\rho_{mix}}$ | $-\frac{\partial p}{\partial z}+\rho_{mix}g_z+Fs_z$ |
| Turbulent Kinetic Energy | 1 | k | $\frac{\mu_{mix}+\frac{\mu^t}{\sigma^k}}{\rho_{mix}}$ | $G_T-\rho_{mix}\varepsilon$ |
| Dissipation Rate of Turbulent Kinetic Energy | 1 | $\varepsilon$ | $\frac{\mu_{mix}+\frac{\mu^t}{\sigma^\varepsilon}}{\rho_{mix}}$ | $\frac{\varepsilon}{k}\left(C_1G_T-C_2\rho_{mix}\varepsilon\right)$ |

Constitutive Equations

$$\mu_{mix}=f_g\mu_g+f_L\mu_L \qquad \rho_{mix}=f_g\rho_g+f_L\rho_L$$

$$G_T=\mu^t\left[2\left(\frac{\partial v_x}{\partial x}\right)^2+2\left(\frac{\partial v_x}{\partial y}\right)^2+\left(\frac{\partial v_x}{\partial y}+\frac{\partial v_y}{\partial x}\right)^2\right]$$

$$\mu^t=C_\mu\cdot\frac{k^2}{\varepsilon}$$

$C_1$, $C_2$, $C_\mu$ model constants $C_e$ transfer coefficient

$$Fs_x=\sigma\kappa\frac{\partial f_L}{\partial x} \qquad Fs_y=\sigma\kappa\frac{\partial f_L}{\partial y} \qquad Fs_z=\sigma\kappa\frac{\partial f_L}{\partial z}$$

Hence, the individual phase continuity equations can be solved to determine the volume fractions, but the individual transport equations can be summed over all phases to give a single transport equation for $\phi_k$. In Table 3 it is possible to identify each term that characterises the 3-D homogeneous model for this specific case.

**Boundary Conditions for the 3-DTHM Model**

The boundary conditions for this case were similar to the 2-DSM model, except for the symmetry condition. Table 4 presents the mathematical form of all boundary conditions.

*Table 4. Boundary conditions for the 3-DTHM model.*

| Boundary Condition | Phase | | |
|---|---|---|---|
| | Mixture | Liquid | Gas |
| Inlet | $v_x\|_{in} = \frac{L}{h_w}\quad v_y\|_{in} = 0\quad v_z\|_{in} = 0$<br>$k\|_{in} = 1.5\left(i \cdot v_x\right)^2$<br>$\varepsilon\|_{in} = \frac{\left(k\|_{x=0}\right)^{1.5}}{0.3\,Ls}$ | $f_l = f_{l,in}$ | $f_g = 1 - f_{l,in}$ |
| Outlet I (Pressure) | $\left.\frac{\partial v_x}{\partial z}\right\|_{outI} = \left.\frac{\partial v_y}{\partial z}\right\|_{outI} = \left.\frac{\partial k}{\partial z}\right\|_{outI} = \left.\frac{\partial \varepsilon}{\partial z}\right\|_{outI} = P_{ref}$ | $\left.\frac{\partial f_l}{\partial z}\right\|_{outI} = 0$ | $\left.\frac{\partial f_g}{\partial z}\right\|_{outI} = 0$ |
| Outlet II (Pressure) | $\left.\frac{\partial v_x}{\partial x}\right\|_{outII} = \left.\frac{\partial v_y}{\partial x}\right\|_{outII} = \left.\frac{\partial k}{\partial x}\right\|_{outII} = \left.\frac{\partial \varepsilon}{\partial x}\right\|_{outII} = P_{ref}$ | $\left.\frac{\partial f_l}{\partial x}\right\|_{outII} = 0$ | $\left.\frac{\partial f_g}{\partial x}\right\|_{outII} = 0$ |
| Wall | $v_x\|_{wall} = v_y\|_{wall} = k\|_{wall} = \left.\frac{\partial \varepsilon}{\partial y}\right\|_{wall} = 0$ | $\left.\frac{\partial f_l}{\partial \zeta}\right\|_{wall} = 0$ | $\left.\frac{\partial f_g}{\partial \zeta}\right\|_{wall} = 0$ |
| $\zeta$ is the orthogonal direction to the wall. | | | |

Figure 2 presents a schematic drawing of the geometry showing the boundary conditions of the 3-D domain.

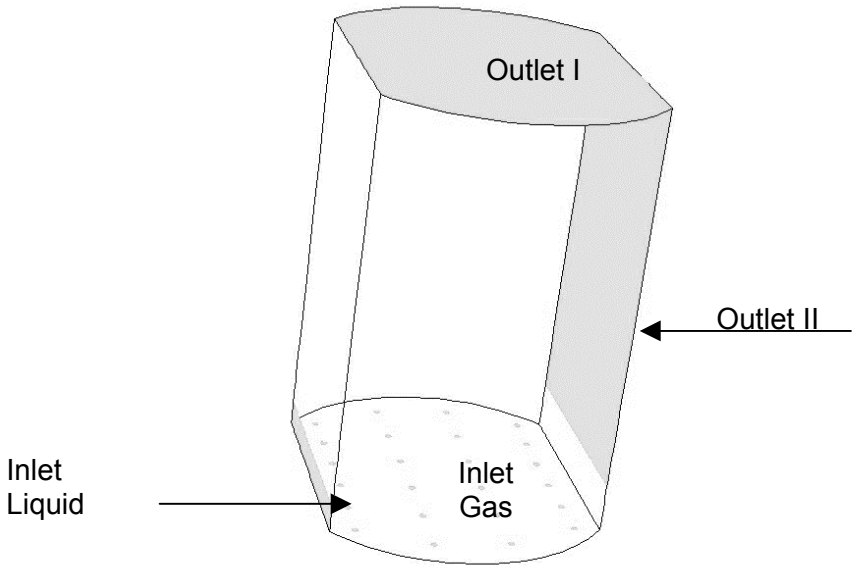


*Figure 2. Specification of the computational domain used in the CFD simulations.*

## NUMERICAL METHODS AND SOLUTION STRATEGY

In a general form, the numerical methods used to solve the models were the finite volume methods (FVMs) with a structured multi-block grid, generated by the body fitted on a generalized coordinate and collocated system. The pressure velocity coupling was the SIMPLEC algorithm with interpolation schemes of first and higher order, UPWIND and HIGHERUPWIND schemes, respectively, to analyse numerical diffusion problems. The Rhie Chow algorithm with the AMG solver procedure was also used to improve the solution and to avoid numerical errors like check-boarding and zigzag due to the use of collocated grids and numerical errors due to non-orthogonal cells generated during the construction of structured grids. Transient solution was also obtained by using an implicit integration method like backward difference with quadratic approximation. The last algorithm is necessary to avoid integration errors when large time steps and end time are used. Tests with the surface sharpening algorithm were carried out to evaluate its influence on the numerical solution. More details on the numerical methods can be found in the CFX 4.4 User Guide [7].

All calculations of this work were performed on a PC like Pentium with Windows® NT operational system, and with an acceptable CPU time.

### Grid Generation

The pre-processor BUILD from CFX 4.4 was used to generate the numerical grid to represent the geometry in the computational domain. Figure 3 shows the sieve plate geometry with diverse blocks and interblock created to obtain a grid with a good orthogonality, for both models: 2-DSM model and 3-DTHM model, respectively. The circular regions are the holes in the plate, defined as inlet gas paths for application of the boundary conditions.

### Post-processing Techniques

The post-processing ANALYSES from CFX 4.4 was used to visualise the main characteristics of the two phase flow. Vector plots, colour maps and animations permit the complete evaluation of the fluid dynamics phenomena under the sieve plate with a good sense of reality, proving that the CFD techniques are a powerful tool to optimise chemical processes.

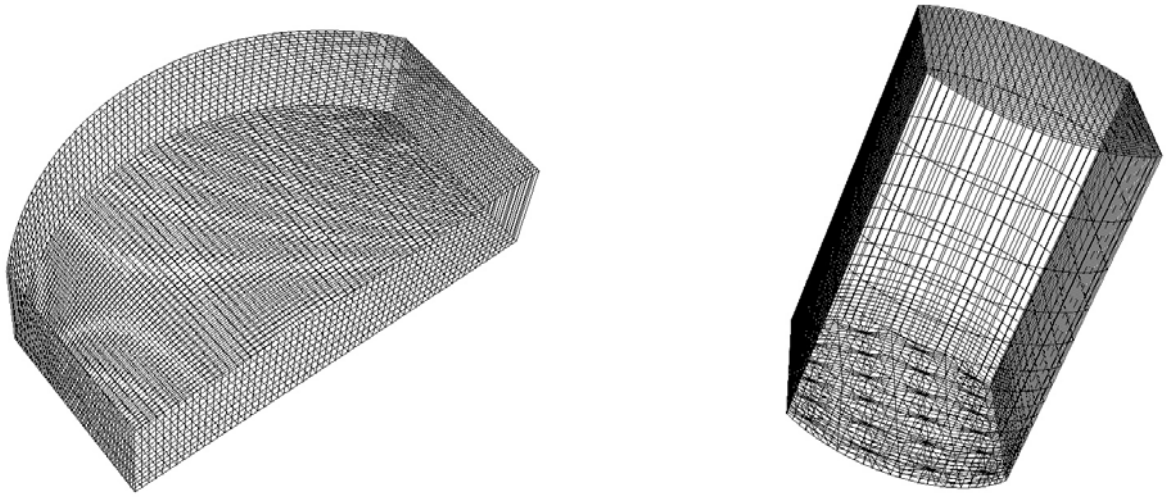

*Figure 3. Numerical grids for the 2-DSM and the 3-DTHM models, respectively.*

## TEST CASES AND RESULTS

According to the objectives of this work, two test cases were chosen to evaluate the capacity of the homogeneous model in representing the vapour-liquid turbulent flow: two phase flow in a bubble column and two phase flow in a stage of a distillation column. In the first one, attention was concentrated on the numerical strategies to get convergence and stability of the numerical solution, and also on the well representation of the bubbles plume in the bulk of the liquid phase. In the other case, the applicability of the single and homogeneous model was tested on the representation of the main fluid dynamics phenomena in the stage of distillation column, such as circulating zones, preferential ways, phase separation and turbulence intensity, among others.

**Case 1: Single Bubble Column**

A small physical model for the bubble column was built up to supply experimental information for the CFD study, and also to permit the physical visualisation of the bubbles plume. Table 5 presents the geometrical and operating parameters used in the test case.

The grid, for this case, can be seen in details in Figure 4. Note the higher concentration of seeds near the symmetry axis of the bubble column (radial direction), and a two ways bias in the distribution of the seeds on the axial direction. This procedure guarantees a good convergence rate in the numerical solution.

During the simulations an experimental study, carried out in a single bubble column, was developed in order to be possible a comparison between scientific visualisation of the flow from CFD computations and photographs obtained by a digital camera. Figure 5 presents frames in different time steps, where it is possible to identify the development of the two phase turbulent flow.

Simulations of the turbulent gas-liquid flow were performed with different numerical strategies to guarantee stability and convergence of the numerical solution. The best way found to minimise numerical errors as numerical diffusion, numerical delay in the transient solutions, etc, typical in CFD calculations, it was to solve the equations of

the model according to the following methodology: by using no under-relaxation factors; with a time integration method composed by backward difference and a quadratic approximation scheme; and finally, dealing the numerical diffusion with a high order (higher upwind) instead of first order (upwind) interpolation schemes.

*Table 5. Geometrical and operating conditions of the bubble column case.*

| Parameter | Bubble Column Case |
|---|---|
| Geometrical | H= 0.38 m (column height) |
| | D= 0.05 m (column diameter) |
| | d= 0.001 m (orifice diameter) |
| Operational | $Q_g$ = 1.00 l/min (volumetric flux of the gas) |
| | $h_w$ = 0.25 m (liquid height) |
| | T = 25 $^oC$ (room temperature) |
| Grid | $N_{cell}$: 16,416 (Number of cells)<br>$N_{block}$: 1 (Number of blocks) |

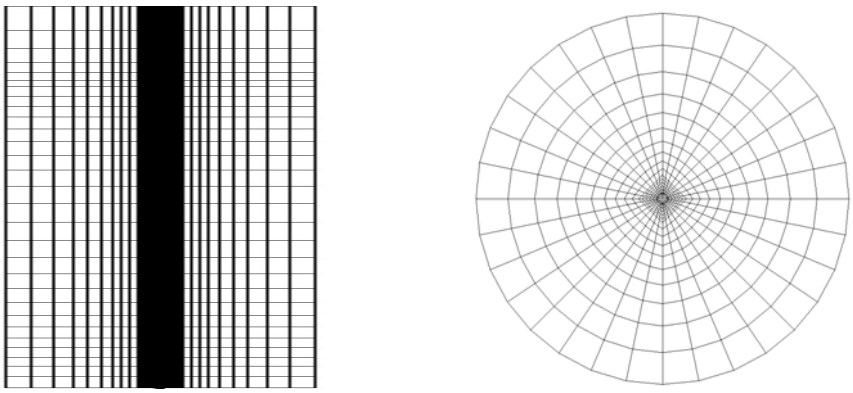

*Figure 4. Bubble column grid.*

Figures 6 and 7 illustrate the dynamic behaviour of the single bubble column obtained by solution of the model with higher upwind and upwind interpolation schemes, respectively. It can be seen small differences in the representation of the gas volume fraction during the development of the flow. Probably, this has occurred due to numerical diffusion errors provoked by the upwind scheme, which reduce the radial velocity and, consequently, the momentum transfer in the radial direction.

By comparison between Figures 5 and 6, it is possible to identify a similar fluid dynamic behaviour. In fact, that observation proves a satisfactory capacity of the homogeneous model, in the representation of the gas-liquid turbulent flow in a single bubble column, despite its assumptions. The complete animation of the flow for several cases is available on our web site: http://www.lfc.furb.br.

Some tests with sharpening surface algorithm, available in the CFX 4.4 CFD code for smoothing of free surfaces, were carried out and a negative effect was produced in the development of the gas-liquid flow. Visualisation of this can be seen in Figure 8.

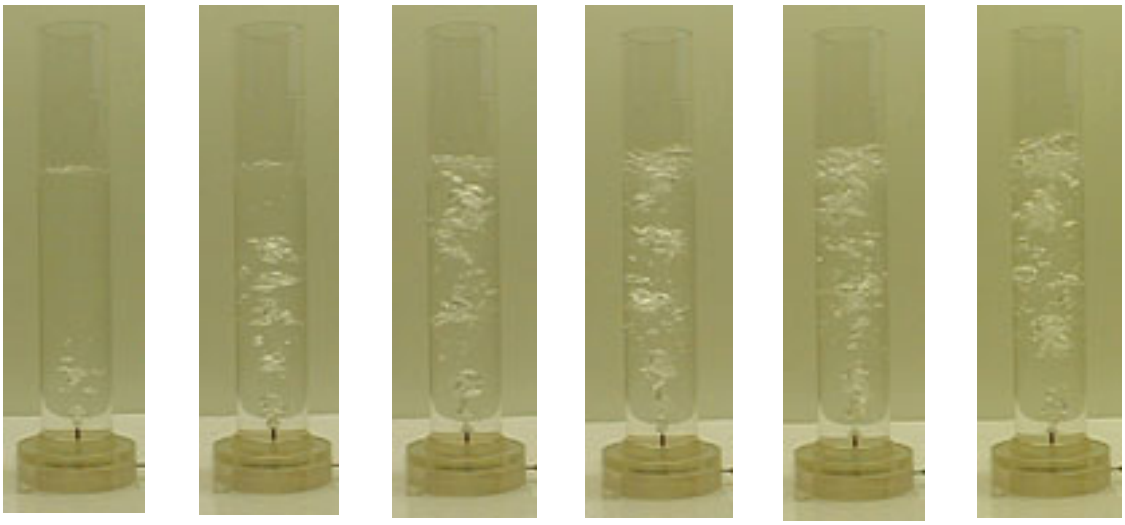

*Figure 5. Pictures of the experimental bubble column.*

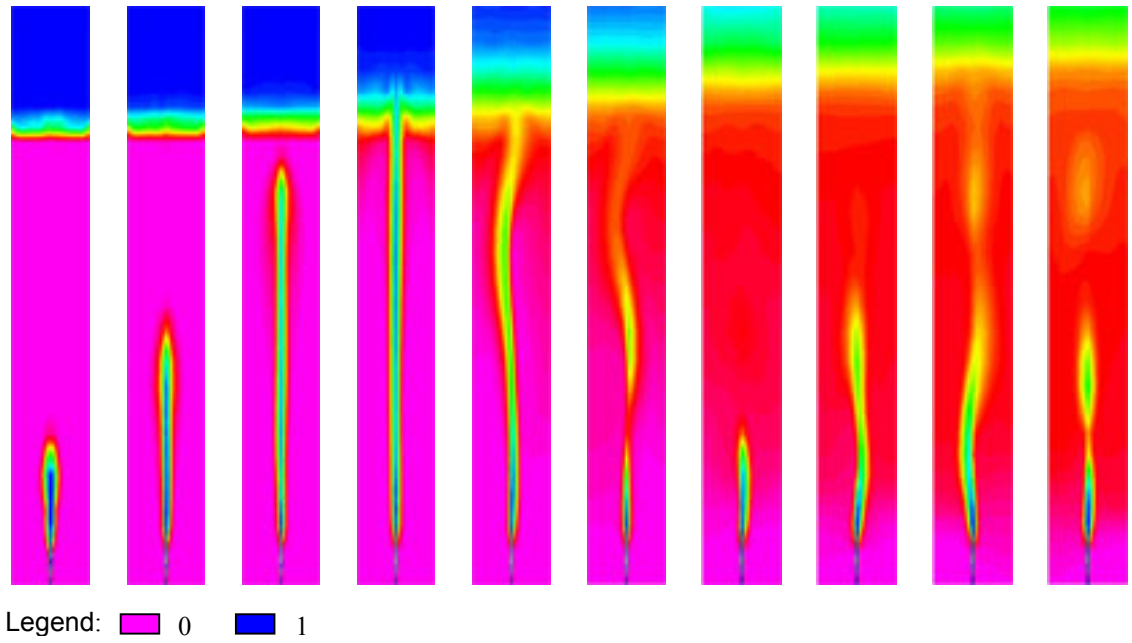


*Figure 6. Maps of the transient behaviour of gas volume fractions (from 0 to 1) obtained with higher order interpolation scheme (higher upwind scheme) for 10 seconds of real time.*

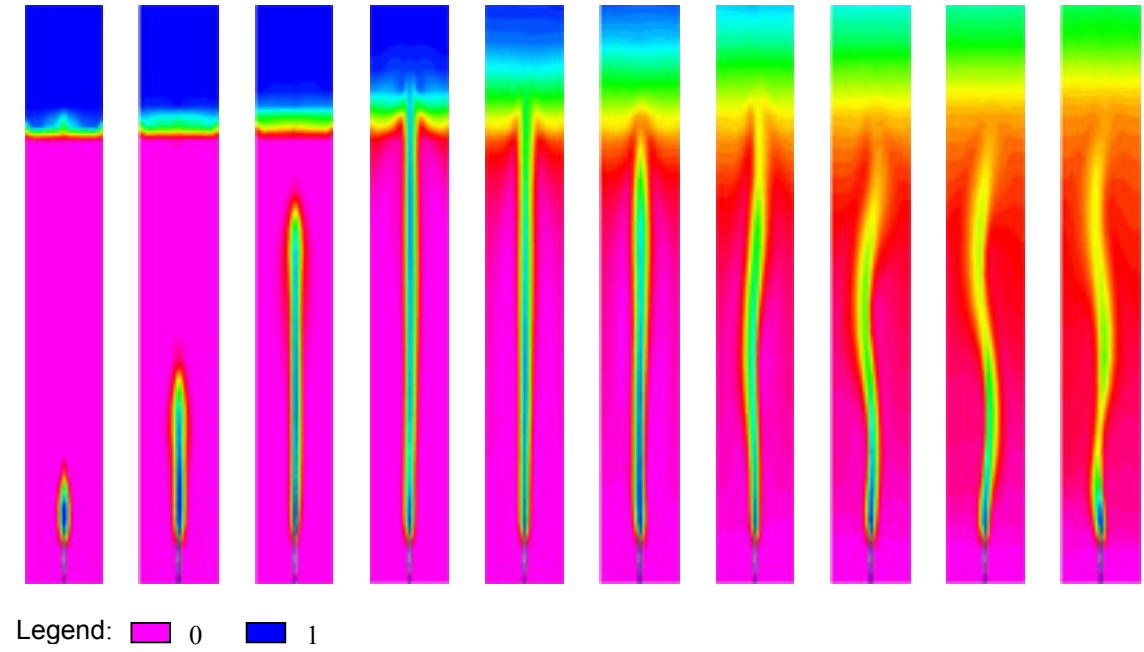


*Figure 7. Maps of the transient behaviour of gas volume fractions (from 0 to 1) obtained with first order interpolation scheme (upwind scheme) for 10 seconds of real time.*

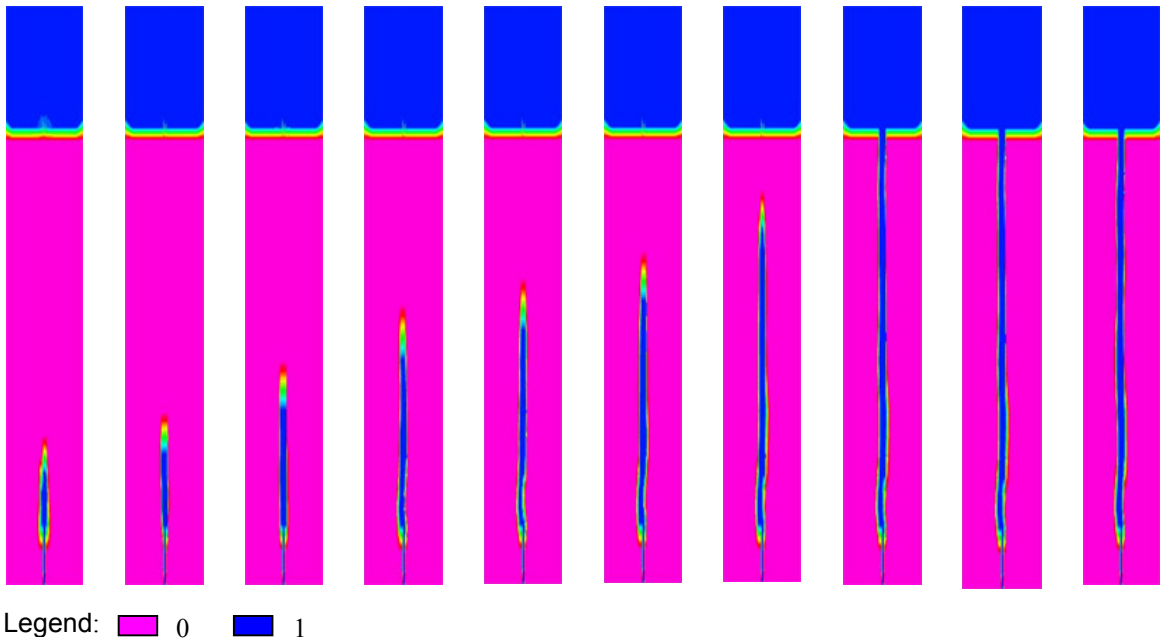


*Figure 8. Maps of the transient behaviour of gas volume fractions obtained with higher order interpolation scheme and making use of a sharpening surface algorithms for 10.0 seconds of real time.*

**Case 2: Sieve Plate Distillation Column**

The sieve plate case was used in this work to compare the two models above mentioned and to analyse the capacity of the homogeneous model to describe the fluid dynamic behaviour of the 3-D sieve plate stage. Table 6 presents the main parameters used in this case.

Firstly, a comparison of the two models was made using Case a of Table 6. Figures 9 and 10 show the grid for both models built up with geometrical characteristics also presented in Table 6.

*Table 6. Geometrical and operating conditions of the sieve plate.*

| Parameter | | Case a | Case b |
|---|---|---|---|
| **Geometrical** | Stage height, m | 0.0630 | 0.0630 |
| | Column diameter, m | 0.0510 | 0.0510 |
| | Hole diameter, m | 0.0008 | 0.0008 |
| | Number of holes | 24.0000 | 24.0000 |
| **Operational** | Volumetric flux of the gas ($x10^6$), $m^3/s$ | 8.4444 | 0.7389 |
| | Volumetric flux of the liquid ($x10^6$), $m^3/s$ | 9.1420 | 1.4844 |
| | Liquid height, m | 0.0070 | 0.0070 |
| | Room temperature, (°C) | 25.0000 | 25.0000 |
| **Grid** | $N_{cell}$: (number of cells) | 23,520 | 23,520 |
| | $N_{block}$ (number of blocks) | 1 | 1 |

The number of cells for the 2-DSM model was 3,600 cells with a CPU time of about 15 minutes, and 23,520 cells with 120 minutes for the 3-DHTM model. Even considering the number of cells, the difference in CPU time was not so large as the expected between the two models. Probably, this occurs because the convergence rate for the steady state turbulent flow is slower in comparison with the transient turbulent flow.

Figures 11 and 12 show maps of pressure and vector plot in a plane on the sieve plates. Despite the fact that the effects of the gas in the liquid flow is included in the 2-DSM, it is not possible to predict small circulating zones that appears in real sieve plates. However, the 3-DHTM model predicts circulating zones more realistically. Besides, the 2-DSM model presents large dependence with an empirical parameter as discussed in details in [4].

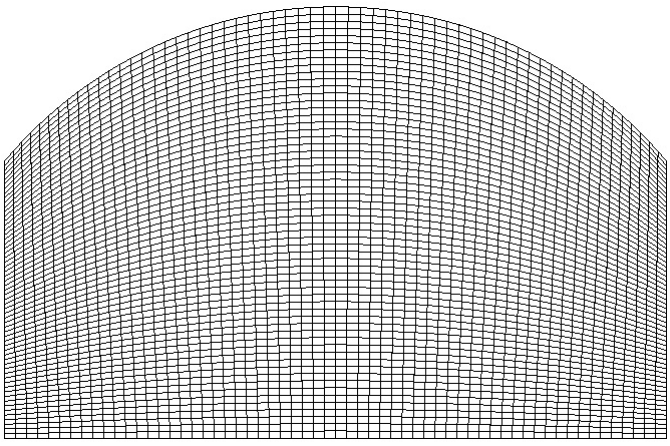

*Figure 9. 2-D grid for the 2-DSM model.*

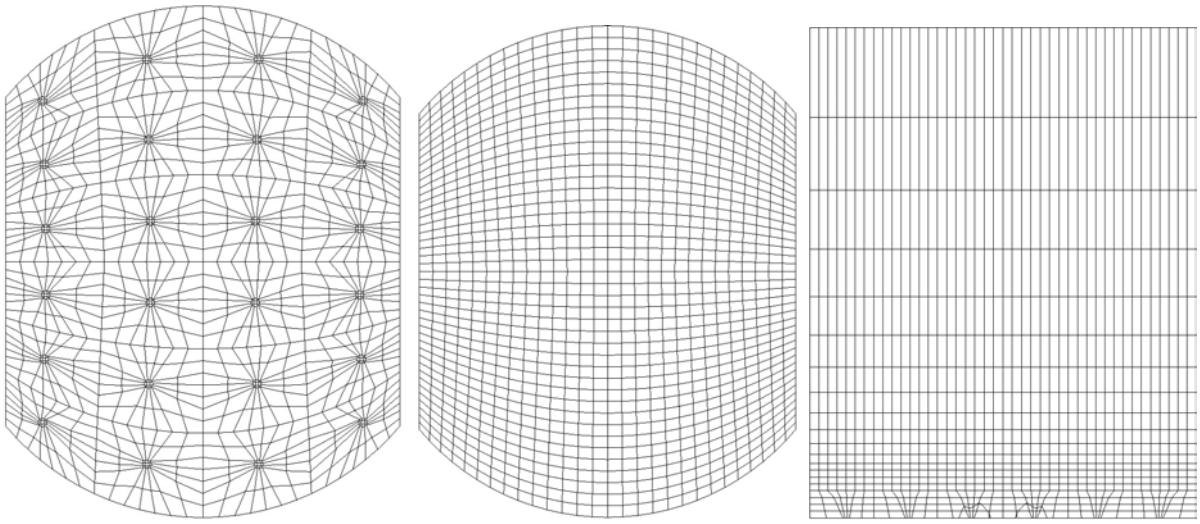

*Figure 10. Planes of the 3-D grid for the 3-DHTM model.*

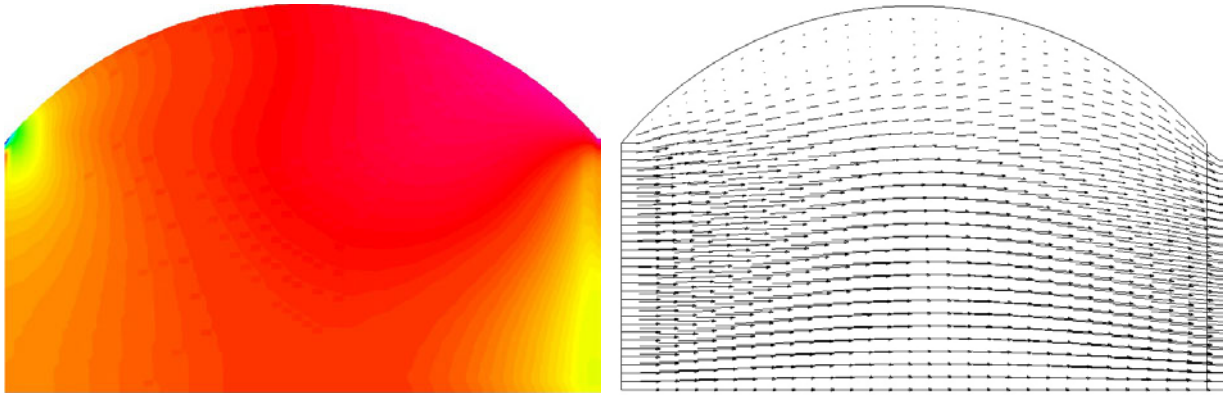

*Figure 11. Map of pressure and vector plot for the 2-DSM model in Case a.*

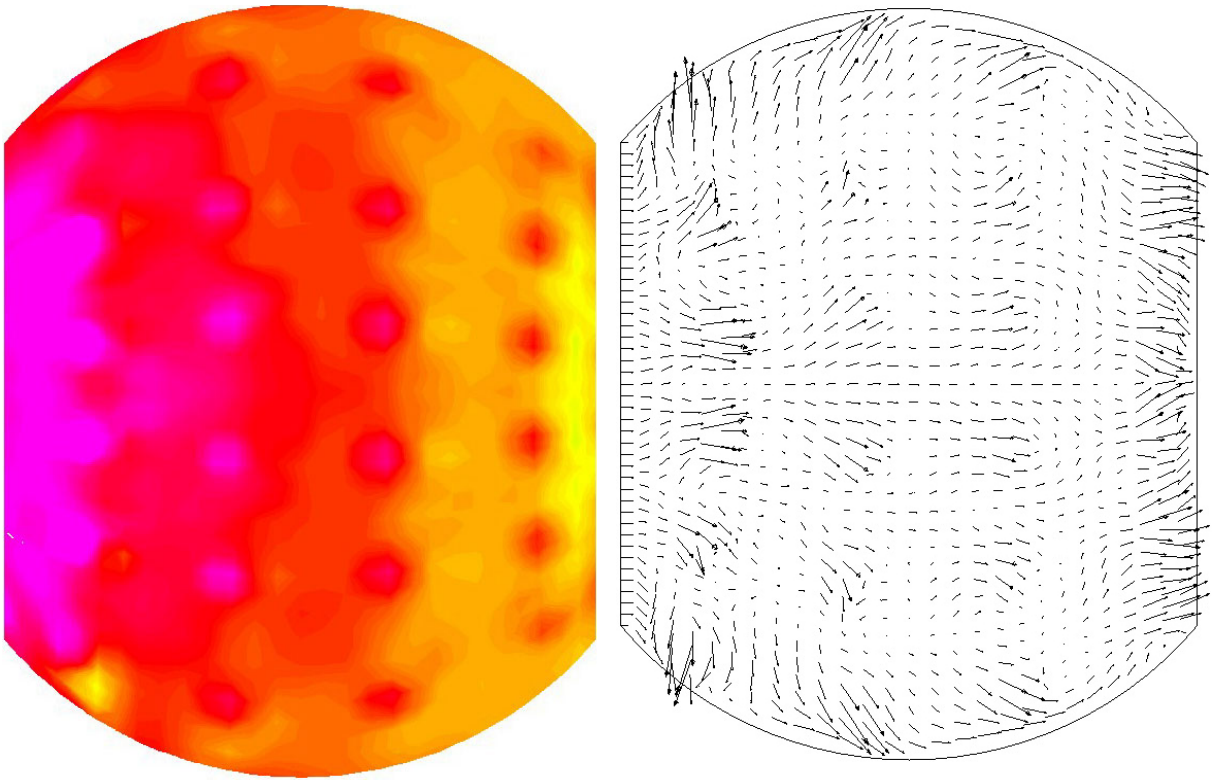

*Figure 12. Map of pressure and vector plot for the 3-DTHM model in Case a.*

With the purpose of analyse the capacity of the homogeneous model to predict the fluid dynamic behaviour of the 3-D sieve plate stage, Figures 13, 14 and 15 show the dynamic of the gas volume fraction from the initial condition (the sieve plate filled with water) to the steady state condition, for both cases (a and b). It was possible to observe the development of a clear liquid height in about 5 seconds of real time for Case a, and in about 8 seconds of real time for Case b.

The difference between Figures 13 and 14 is related with the change in the volumetric fluxes of the gas and the liquid phases. A top view of the dynamic of Figure 13 (Case a) is shown in Figure 15.

The complete animation is available on our web site: http://www.lfc.furb.br.

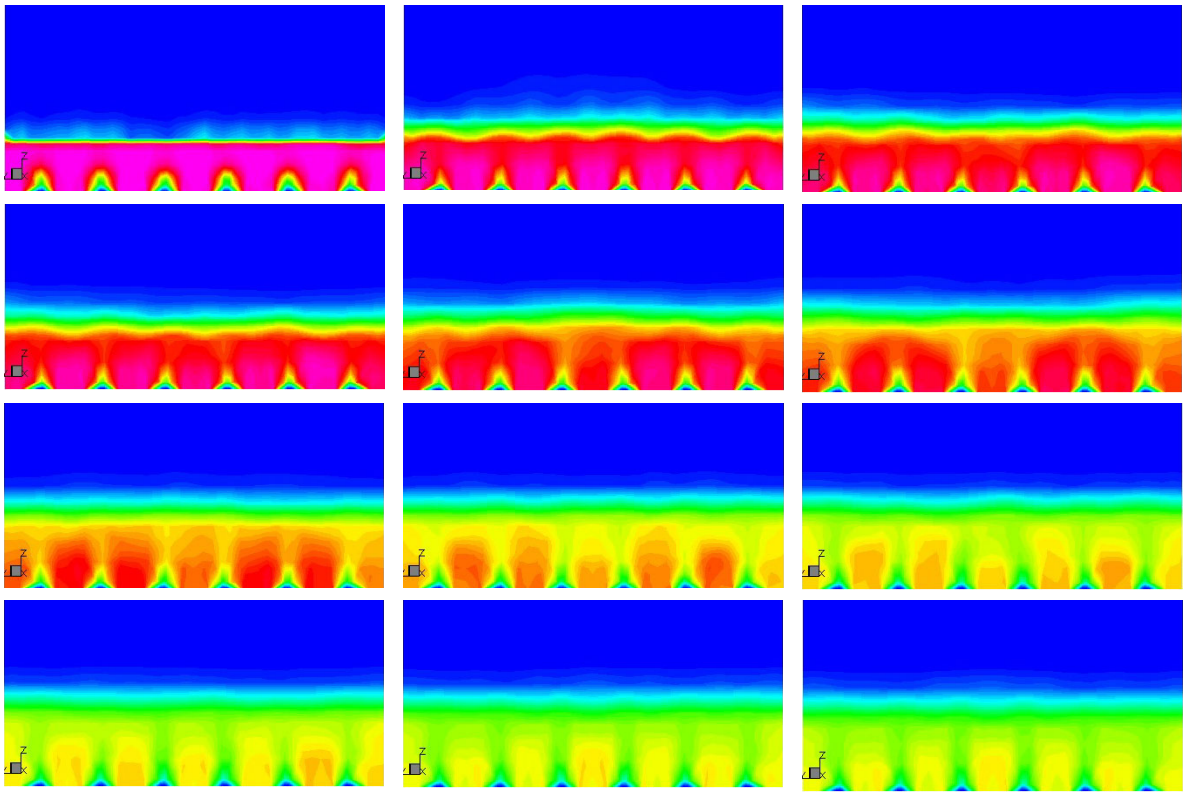

*Figure 13. Dynamic of gas volume fraction for Case a in 6 seconds of real time.*

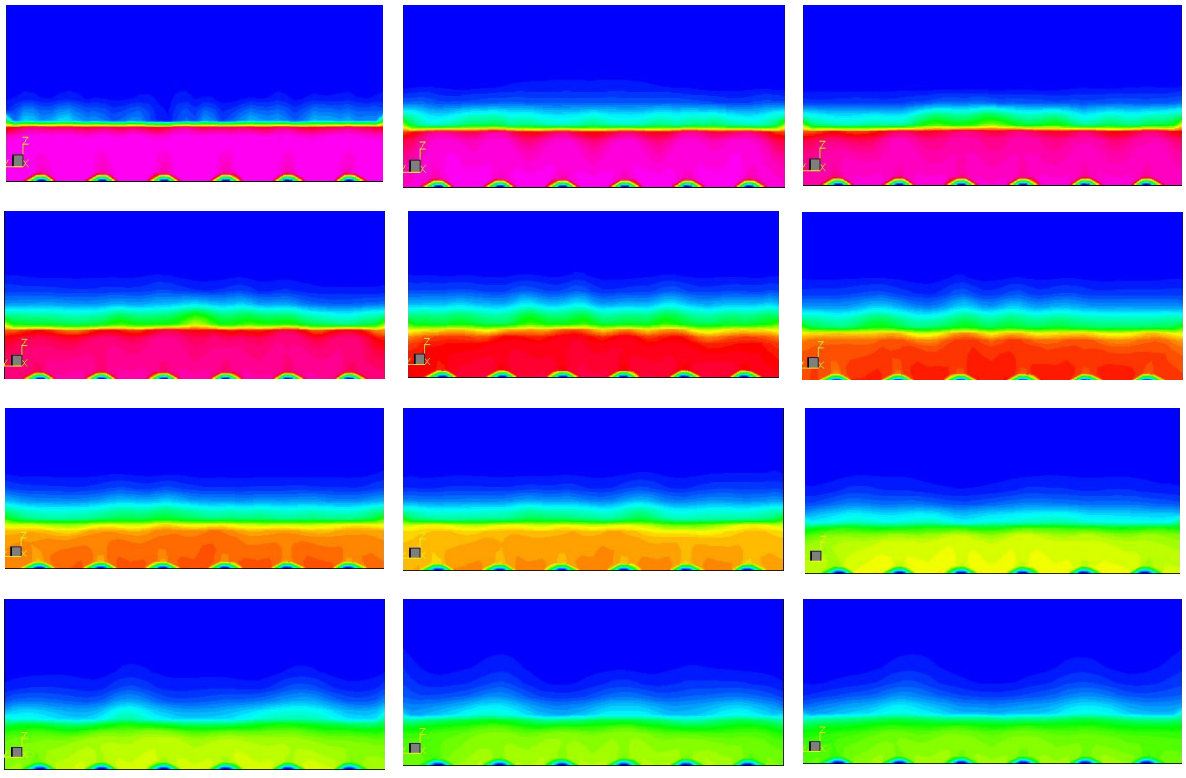

*Figure 14. Dynamic of gas volume fraction for Case b in 10 seconds of real time.*

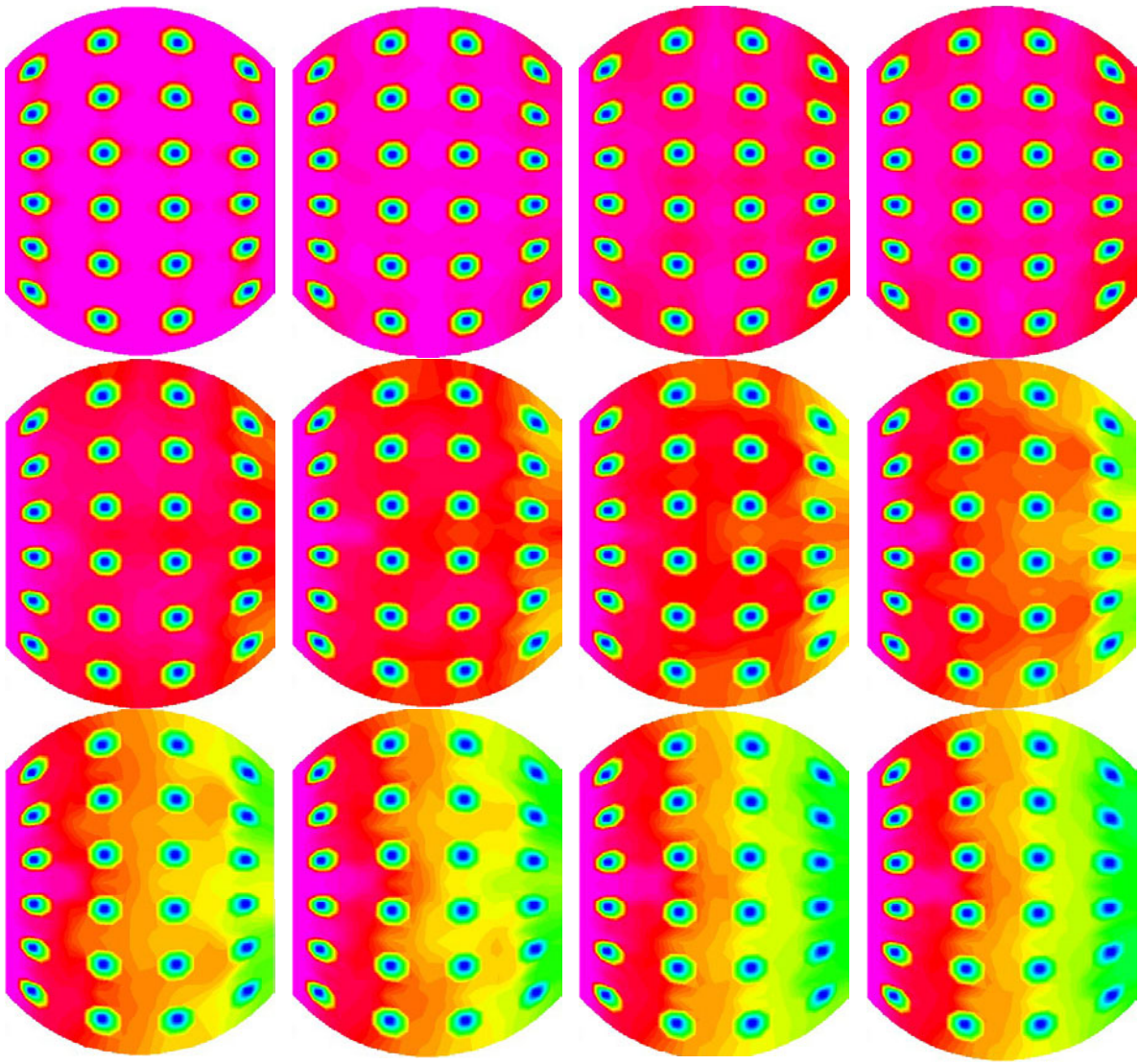

*Figure 15. Top view of dynamic of gas volume fraction for Case a in 6 seconds of real time.*

## CONCLUDING REMARKS

The main conclusions of this work can be summarised as:

- the comparison between the models presented shows that the 3-D homogeneous model is more realistic than the 2-D single model in the representation of the fluid dynamic of the gas-liquid flow on a sieve plate of a distillation column;
- the computational efforts is large for both models, but the transient solution presents more stability and convergence rate;
- numerical diffusion can be found when first order interpolation scheme is used and no under relaxation factors can be used to achieve a transient solution;
- the CFD tools presented and discussed in this work make possible to know better the turbulent gas-liquid flow on a sieve plate of a distillation column and they can be used to optimise the design and operating condition of distillation column;

- and finally, the next step of this work is to extend the experimental work using a sieve plate with 360 mm in diameter, with experimental data obtained from hot fire anemometer system.

## ACKNOWLEDGEMENTS

The authors would like to acknowledge the financial support received from FAPESP (Fundação de Amparo à Pesquisa do Estado de São Paulo) grant n$^{o.}$ 01/01987-6 and FINEP (Financiadora de Estudos e Projetos) grant n$^{o.}$ 65.00.0274.00.

## NOMENCLATURE

Latin Letters

| | |
|---|---|
| $C_{\mu,}$ | |
| $C_1$, $C_2$ | model constants |
| Ce | transfer coefficient |
| D | column diameter, m |
| d | holes diameter, m |
| f | volume fraction and resisting force acting on the flowing liquid |
| **Fs** | surface tension vector, N/m |
| G | generation of turbulence |
| **g** | gravitational acceleration vector, m/s$^2$ |
| h | clear liquid height, m |
| H | column height, m |
| $h_w$ | weir height, m |
| k | turbulent kinetic energy, m$^2$/s$^2$ |
| L | rate of liquid flow, m$^3$/s m |
| $L_s$ | dissipation length scale, m |
| N | number |
| P | pressure, Pa |
| Q | volumetric flux, m$^3$/s |
| S | source term |
| T | room temperature, ºC |
| t | time, s |
| $U_s$ | superficial velocity of gas , m/s |
| **v** | velocity vector, m/s |
| x | co-ordinate, m |
| y | co-ordinate, m |
| z | co-ordinate, m |

Greek Letter

| | |
|---|---|
| $\rho$ | density, kg/m$^3$ |
| $\phi$ | fluid dynamic properties (u, v, w, k and $\varepsilon$) |
| $\Gamma$ | diffusion coefficient |
| $\sigma^{\varepsilon}$, $\sigma^{k}$ | constant of k - $\varepsilon$ model |
| $\varepsilon$ | dissipation rate of turbulent energy, m$^2$/s$^3$ |
| $\mu$ | viscosity, kg/m s |
| $\zeta$ | orthogonal direction to the wall |

Subscripts

| | |
|---|---|
| g | referring to gas phase |
| in | referring to inlet region |
| k | index referring to one of the two phases |
| L | referring to liquid phase |
| mix | mixture properties |
| out, out I, out II | referring to outlet region |
| T | turbulence |
| x | referring to x direction |
| y | referring to y direction |
| z | referring to z direction |

Superscript

| | |
|---|---|
| eff | effective properties |
| t | turbulence |

## REFERENCES


1. B. Mehta and K. T. Nandakumar (1998), Chem. Eng. Res. and Design, Trans. I. Chem. E. 76, 843-848.

2. C. J. Liu, X. G. Yuan, K. T. Yu and X. J. Zhu (2000), Chemical Engineering Science, 55, 2287-2294.

3. J. M. van Baten and R. Krishna (2000), Chemical Engineering Journal, 77, 143-151.

4. C. Soares, D. Noriler, M. R. Wolf-Maciel, D. Santos, A. A. C. Barros and H. F. Meier (2001), 22nd Iberian Latin-American Congress on Computational Methods in Engineering, Campinas, São Paulo, Brazil, 17 pp.

5. M. Q. Zhang and K. T. Yu (1994), Journal of Chemical Engineering, 2, 63-71.

6. K. E. Porter, K. T. Yu, S. Chambers and M. Q. Zhang (1992), IChE Symposium Series, 128, A257-A273.

7. CFX-4 for Windows NT. CFX-4.4 User Guide. AEA Technology. Oxfordshire, United Kingdom, 2001.